Nuclear Materials and Energy 24 (2020) 100779

Contents lists available at ScienceDirect

Nuclear Materials and Energy

journal homepage: www.elsevier.com/locate/nme

# Exposures of bulk W and nanostructured W coatings to medium flux D plasmas

M. Sala[a,*], A. Uccello[b], D. Dellasega[a,b], M. Pedroni[b], E. Vassallo[b], M. Passoni[a,b]

[a] Politecnico di Milano, Department of Energy, Milan 20133, Italy
[b] Istituto per la Scienza e Tecnologia dei Plasmi, CNR, Milan 20125, Italy

ARTICLE INFO

*Keywords:*
Nanostructures
Tungsten
D plasmas exposures

ABSTRACT

In this work, we discuss the exposures of polycrystalline tungsten (W) and nanostructured W coatings to high energy (~30 ÷ 300 eV) medium-flux D ($\sim 10^{20}\,m^{-2}s^{-1}$) deuterium plasmas of the linear machine GyM at an overall fluence of $10^{24}\,m^{-2}$. The energy and particle flux are tailored to that of charge-exchange neutrals at the vessel main chamber of present-day tokamaks and expected in ITER. Scanning Electron Microscopy measurements show the formation of surface nanostructures that are found to strongly depend on the W morphology and crystallinity, as well as on the energy of the ion species. The obtained nanostructures are few nanometres deep and similar to the one obtained after exposure of bulk W to divertor-like conditions. Dedicated annealing experiments are performed on selected samples, showing that the nanostructures developed on W coatings are thermally stable up to their recrystallisation temperature. The development of micrometric-sized blisters is also observed and found to strongly depend on the features of the W coatings, the substrate and the applied bias voltage.

## 1. Introduction

Due to its favourable thermophysical properties, tungsten (W) has been chosen as a reference material for the most critical plasma facing components (PFCs) in ITER [1]. The performances of W as a first wall material have been demonstrated in several tokamaks as well as in laboratory experiments, such as linear plasma machines and ion beam loading devices [2,3]. However, due to plasma-wall interactions (PWIs), W PFCs can be eroded, leading to prompt W redeposition in the divertor region, or to a mixing of W with other plasma impurities (such as nitrogen) and the formation of co-deposits on top of the pristine first wall [4–6]. The co/re-deposited layers are usually characterised by different morphology, structure, composition and thickness with respect to bulk materials, depending on the type of first wall materials, the specific location in the machine and the history of all the operating tokamak conditions. Both the pristine PFCs and the co/re-deposits are subject to low energy (tens of eV) intense particle fluxes (up to $\sim 10^{24}\,m^{-2}s^{-1}$) in the divertor region. Fusion-relevant plasma exposures of both bulk (polycrystalline) W and W coatings are usually performed in linear machines, compact and cost-effective devices capable of producing plasmas with particle fluxes similar to those present in the different regions on the first-wall of both present day tokamaks and ITER.

More specifically, polycrystalline (bulk) W modifications at the micro/nano scale has been reported in literature after exposures to pure deuterium (D) plasmas in divertor-like regimes [7–12]. The formation of surface nanostructures in form of ripples, triangles and sponges have been reported [9,8] and they have been correlated with different crystallographic orientation of the W grain. In addition, the formation of nanometric-sized D bubbles have been reported in [11]. Exposures of W coatings instead of bulk W affects the features of the obtained morphology. In [13] different types of W coatings deposited on bulk W (columnar, nanocrystalline and amorphous-like W), were exposed to divertor-like plasma in Pilot-PSI. The nanostructures formed on columnar W were similar to the ones of bulk W being related to the orientation of the underlying W grains. On the other side, nanocrystalline and amorphous-like W films, due to their different structure, exhibited a new mixed morphology not related to the W grains of the substrate. W modifications at the nanoscale can have important impact on PWI in tokamak devices. Indeed, it has been shown that they can lead to enhanced hydrogen retention [7]. In addition, PWI processes such as sputtering occur at the surface of PFCs and, thus, they can be deeply influenced by morphological modification of the exposed surfaces.

Alongside nanostructures, D plasma exposures of W also show the formation of micrometric-sized blisters, which were observed in each of the above-mentioned works. The formation of blisters on polycrystalline W after fusion-relevant D exposures has also been investigated in

* Corresponding author.
*E-mail address:* michele.sala@polimi.it (M. Sala).

https://doi.org/10.1016/j.nme.2020.100779
Received 6 March 2020; Received in revised form 13 July 2020; Accepted 14 July 2020
Available online 29 July 2020

depth with respect to both the impinging ion energy, fluence, surface temperature and roughness [14–19]. Blisters formation on W surfaces can lead to an increase D retention of plasma-exposed surfaces [8]. In addition, blisters can burst leading to the release of impurities within the plasma [20].

Surface modifications at the nano/micro-scale have been extensively investigated in literature. However, these studies usually focus on W, exposed to plasmas with low energy (~40 eV) of the ion species and with fluxes which are typical to those present at the divertor of present-day tokamaks (~$10^{22\div24}$ $m^{-2}s^{-1}$). Much less attention has been instead paid to the behaviour of W after the exposures to medium flux ($10^{20}$ $m^{-2}s^{-1}$) and high energy (>100 eV) D plasmas. D plasmas with these characteristics mimic charge-exchange neutrals (CXNs) fluxes at the main chamber of both present-day tokamaks [21,22] and ITER [23,24]. PWI studies concerning exposures to CXNs-like plasmas are related to ITER main chamber or structural materials such as beryllium and Eurofer, and usually focus on D retention and erosion (e.g. [25–27]). On the other hand, modifications at the nano/micro-scale of bulk W and nanostructured W coatings due to CXNs-like fluxes in a full-W DEMO-like scenario have not been addressed. It is thus of interest to study the modifications of W at both the nanoscale (formation of nanostructures) and the mesoscale (formation of blisters) in the peculiar regime of CXN-like plasma fluxes and ion energies and compare them with the above-mentioned literature results.

In this work, polycrystalline (bulk) W and W coatings having different morphology, structure, crystallinity and composition produced via the Pulsed Laser Deposition (PLD) technique were exposed to the medium flux deuterium plasma in the linear plasma device GyM, tuning the energy of the impinging ion species in the range of 20 ÷ 300 eV by properly biasing the samples holder. The W coatings were deposited on flat Si (100) substrates. The reason for this is to allow for an easier post-exposure analysis of the samples cross-sections, which can be performed by cleavage of the substrate, that is by cutting it along crystallographic directions applying a proper pressure. To address the role of the substrate in the plasma-induced modifications, one of the selected W morphology was also deposited on polycrystalline W and on fine grain graphite. The influence of the substrate materials in the observed plasma-induced modifications is thoroughly discussed in the text. Finally, to separate the combined effects of particle and thermal loads due to the plasma exposures, dedicated annealing experiments were also done on selected nanostructured W morphology.

## 2. Experimental methods

### 2.1. Deposition of W coatings via PLD

The W coatings considered in this work were produced via PLD technique. Details of the coatings production and characterisation can be found in [28,29]. We chose three different nanostructured morphologies: amorphous (a-W), columnar (c-W) and porous (p-W). Only the background gas and pressure were changed in our PLD depositions, as detailed in Table 1, while the laser wavelength, energy per pulse and laser fluence were set to 532 nm 730 mJ and 11.41 J/cm$^2$ in all the depositions. The c-W films mimic the morphology of combined magnetron sputtering ion implantation W-coated tiles in full-W devices such as AUG [30]. The a-W and p-W ones are similar to W-based redeposits found on the FW with high (tens of eV) and low (~1 eV) energies, respectively [31,32]. Flat silicon (100) substrates, 500 μm thick, were chosen to facilitate post-exposure analyses, particularly to characterise the surface nanostructures. For the a-W films, a thin (~100 nm) c-W interlayer was deposited first, in order to improve the adhesion of the film on the Si surface and to mimic the original surface of W-coated tiles on which the redeposited layer might develop. The overall thickness of the coatings, estimated via SEM analysis, was in the range of ~460 nm. To investigate the role of the substrate material and surface roughness with respect to blister formation, the c-W morphology was deposited on mirror-like and rough W and also on mirror-polished Gr, each substrate with a thickness of about ~1 mm. W substrates were given a surface roughness of around 400 nm by a mechanical treatment, which was performed using a lapping machine, changing the grit of the sandpaper.

**Table 1**
PLD background pressure for the deposition of the c-W, a-W and p-W coatings.

| | Background gas |
|---|---|
| c-W | $10^{-3}$ Pa |
| a-W | 70 Pa of He |
| p-W | 50 Pa of Ar |

### 2.2. Characterisation of selected W morphology

The morphology of the as-deposited samples was investigated with a Zeiss Supra 40 field emission scanning electron microscope (SEM) with an accelerating voltage of 5 keV. SEM plain-views and corresponding cross-sectional morphology are shown in Fig. 1. The c-W and the a-W coatings show a compact morphology, while the p-Ws an open one, characterised by a cauliflower-like structure. In the leftmost part of 1, we show a SEM plain view of the polycristalline Plansee W. In Fig. 2, we show SEM images of the c-W coatings deposited on rough W. The crystallinity of the W coatings deposited on Si was investigated via X-ray diffraction (XRD) spectrometry using a Panalytical X'Pert PRO X-ray diffractometer in the $\theta/2\theta$ configuration, as presented in [28]. c-W coatings are characterised by ~16 nm crystallites, while the grains are ~50 nm. The details for these estimation can be found in [28]. The a-W samples present an amorphous structure, with the crysallite size below 2 nm. The roughness (see Table 2) of both the substrates and the as-deposited c-Ws was investigated by means of a NanoRTM Atomic Force Microscope (AFM) in air (Pacific Nanotechnology, Santa Clara, CA, USA). Measurements were taken in contact mode at a scan speed of 0.7 μm/s with a scan size of 70 × 70 μm$^2$.

### 2.3. Plasma exposures in GyM

GyM [33] is a linear machine consisting of a vacuum chamber (diameter 0.25 m, length 2.11 m) mounted inside 10 coils, capable of producing a peak magnetic field of about 0.16 T which confines the plasma column. The plasma is sustained and maintained by a

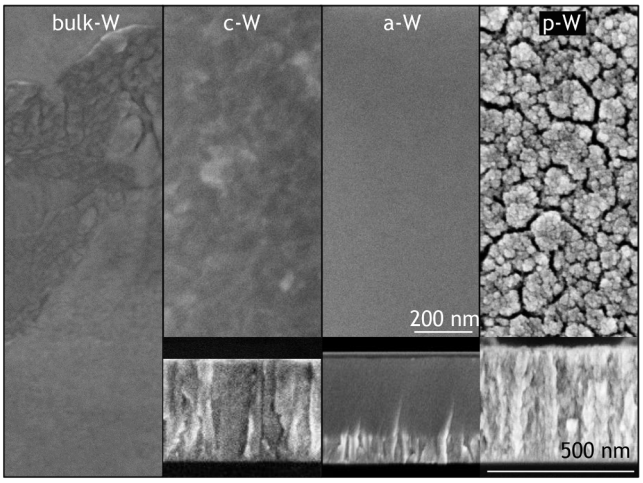


**Fig. 1.** SEM images of the bulk W and the c-W, a-W and p-W coatings deposited on flat Si substrates. The length scale 200 nm is the same for all SEM plain-views. The insets in each subfigure show the cross-sectional morphology.

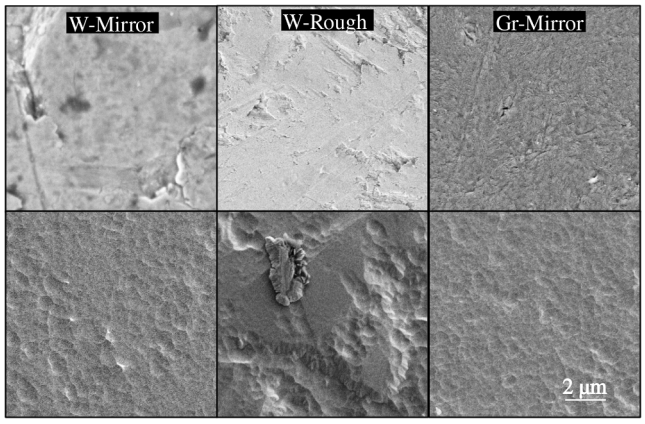


**Fig. 2.** SEM plain views of the W and Gr substrates without coating (top row) and with the c-W film (bottom row) deposited on top. The length scale (2 μm) is the same for all the images. One can see that the coatings follow quite well the substrate topographies, with a comparable average roughness.

**Table 2**
AFM measurments of the substrates and c-W coatings average roughness ($R_a$), measured by AFM over an area of 70 × 70 μm$^2$.

| Substrate | W mirror | W rough | Gr mirror | Si mirror |
|---|---|---|---|---|
| $R_a$ | 95 nm | 500 nm | 95 nm | 0.6 nm |
| c-W coatings | W mirror | W rough | Gr mirror | Si mirror |
| $R_a$ | 75 nm | 527 nm | 69 nm | 0.6 nm |

**Table 3**
Campaign-averaged electron density, electron temperature, plasma potential, ion flux and fluence by the LP located at the machine axis in front of the samples holder.

| $n_e$ [m$^{-3}$] | $T_e$ [eV] | $V_p$ [V] | $\phi$ [m$^{-2}$s$^{-1}$] | $\Phi$ [m$^{-2}$] |
|---|---|---|---|---|
| $6.2 \times 10^{16}$ | 6.8 | 23.7 | $5.1 \times 10^{20}$ | $6.7 \times 10^{24}$ |

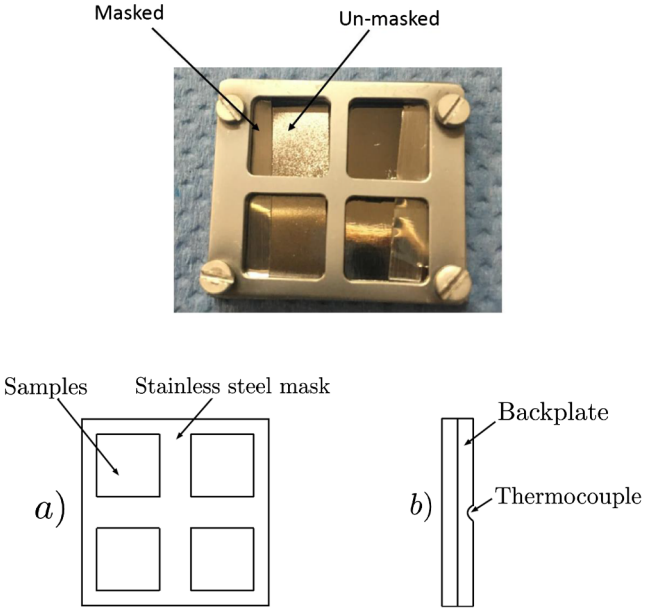


**Fig. 3.** Top: picture of the samples holder, showing the details of the samples preparation before exposures. Bottom: schematic view of the samples holder. *a*) top view; *b*) side view, showing the location of the thermocouple located at the backplate.

magnetron source connected to the vessel through a rectangular waveguide, exploiting the electron cyclotron resonance absorption mechanism at B = 0.0875 T. The main plasma parameters (electron temperature, density and plasma potential) are monitored through a Langmuir Probe (LP). For the exposures performed in this work, the probe was positioned on the axis of the machine ≃ 0.5 m in front of the samples holder. Deuterium was used as the working gas. Campaign-averaged electron density ($n_e$), electron temperature ($T_e$), plasma potential ($V_p$) and particle ion flux ($\phi$) are reported in Table 3. For all the experimental campaign, the exposure time was 4 hours. Together with the measured ion flux reported in Table 3, this led to a fluence ($\Phi$) on the samples of about $6.7 \times 10^{24}$ m$^{-2}$. The samples holder (see Fig. 3) has a stainless steel mask and can accommodate up to four (10 × 10 mm) squared specimens. In order to investigate the modifications induced to the W coatings by the plasma of GyM as a function of the ion energy, different (negative) bias voltages were applied to the samples holder. The bulk W, c-W, a-W and p-W morphology were exposed to the following bias voltages: *i*) no bias, *ii*) −100 V, *iii*) −200 V, *iiii*) −300 V, which correspond to an energy of the impinging ion species on samples in the range 20 eV, 120 eV, 220 eV and 320 eV, respectively. Instead, the c-W deposited on mirror-like and rough W were exposed with no applied bias voltage. For clarity, only the absolute values of the applied bias voltage will be considered in the following. The values of the bias voltages were chosen because the corresponding energy of the ion species are typical of high-energy charge-exchange neutrals impinging on the main chamber of ITER. Moreover, they are, below, around and above the sputtering threshold of Magnetron Sputtering-deposited W (as reported by Sugiyama et al. in [34]), respectively. The samples-holder is water-cooled (~13 °C) and removes the impinging power and after about 30 min of the exposures a steady-state temperature is reached. A thermocouple is located behind the back-plate. The temperature readings are 100°, 120°, 190° and 260 °C for the four bias conditions that we considered in our work. A specific characterisation of the temperature difference between the thermocouple at the back-plate and the surface of the samples was carried on employing an external heating source. The surface temperature was estimated to be higher than that at the backplate by ~120 °C.

## 3. Results

### 3.1. Nanostructures formation

Fig. 4 shows high-magnification SEM plain-views of the exposed W coatings deposited on Si and the bulk W samples at increasing bias voltage. One can notice that no modification at the nanoscale occurs for all the exposed morphology when no bias is applied. For an applied bias voltage of 100 V nanostructures start to develop on the bulk-W. Low-magnification SEM analysis on the bulk-W revealed the formation of three different type of nanostructure (ripple-like, spongy-like and jagged-like), as can be noted from Fig. 5, which are depending with the particular grain considered. The ripple-like nanostructure observed on the bulk-W developed also on the c-W film, while the other two reported in Fig. 5 were not seen in any of our exposures. As it happens for the bulk-W, the ripples are confined within the grains, whose dimension is around 20 nm. Fig. 6 allows to appreciate that the ripple nanostructure is just few nanometers deep. The a-W films showed, instead, the development of a hole-like nanostructure at 200 V. Furthermore, at 300 V one can observe the formation of a ripple-like structure similar to that developed on the bulk-W and c-W coating. Considering finally the p-W films, SEM analysis at the nanoscale revealed no formation of any feature, but rather a progressive smoothing of the surface after the plasma exposure, with coalescence of the original, cauliflower-like morphology. This smoothing effect, observed for applied bias voltages $\geqslant$ 100 V, is related to the progressive erosion of the p-W films, which has

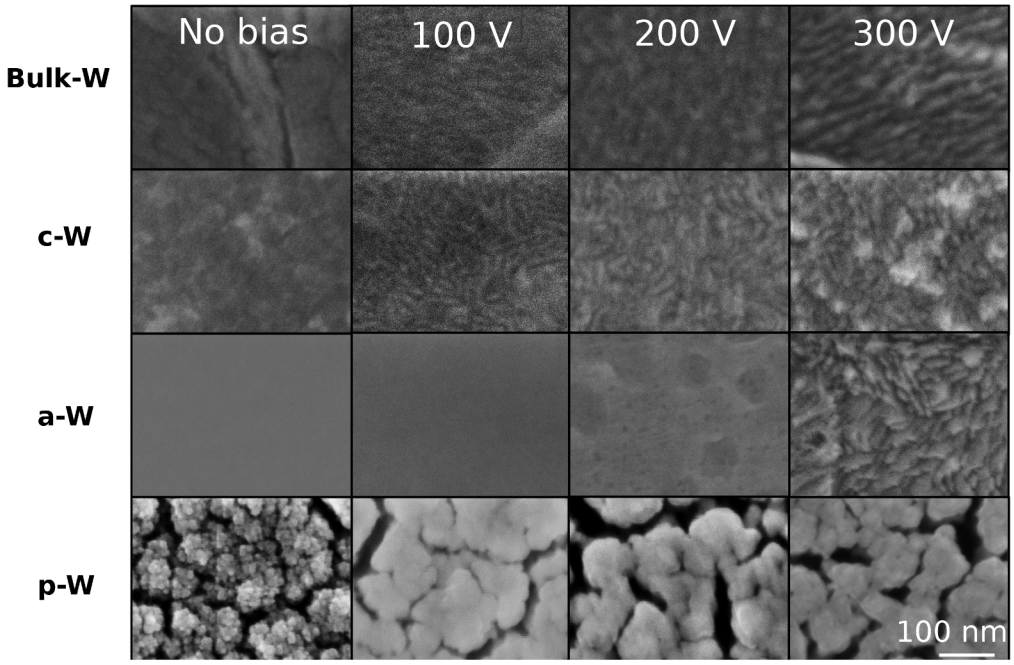


**Fig. 4.** SEM plain views showing a summary of the surface morphology evolution due the irradiation at increasing bias voltages, for bulk W and W coatings deposited on flat Si. The exposure performed with no applied bias voltage showed no induced modifications at the nanoscale.

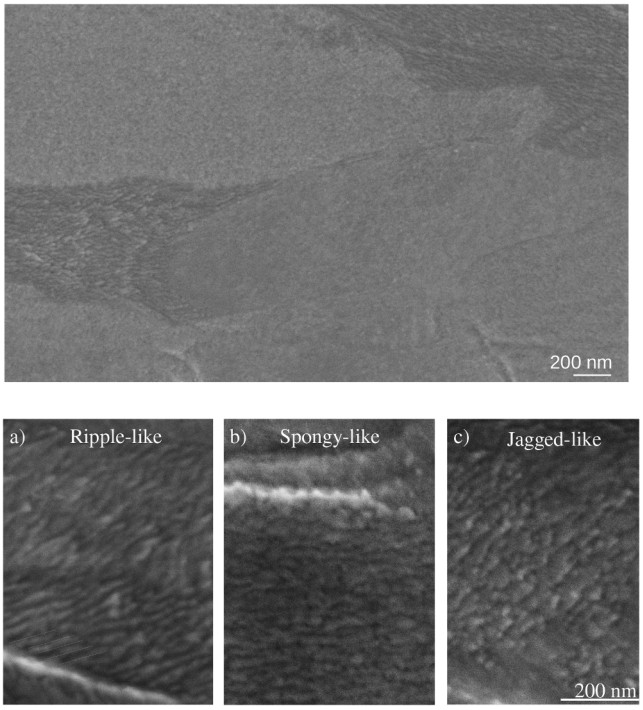


**Fig. 5.** Low magnification SEM plain view (top) of the bulk-W exposed at 300 V, highlighting the strong dependence of surface nanostructures on the crystalline grains. Ripple-like a), spongy-like b) and jagged-like c) nanostructures (bottom) observed on different crystalline grains on the bulk-W exposed at 300 V. White lines are added in figures a) and c) to help appreciate the differences between the ripple and jagged-like nanostructures.

been evaluated by SEM cross-sections of the samples. For the exposures performed at 100 V, 200 V and 300 V we estimated an erosion of about 23.3 nm, 56.7 nm and 69.7 nm respectively. A summary of the observed nanostructures is shown in Table 4.

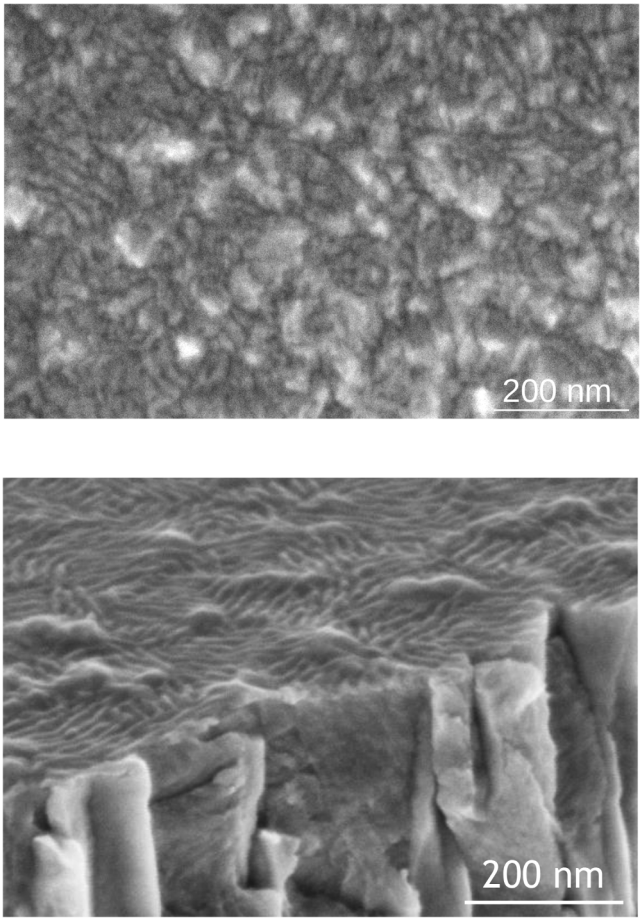


**Fig. 6.** SEM plain view (top) of the c-W exposes at 300 V, showing that the ripple-like nanostructure is well confined within the crystalline grains. Tilted SEM cross-section (bottom) of the c-W exposed at 300 V, showing that the ripple nanostructures are few nanometer deep.

**Table 4**
Summary of the nanostructures observed on the coatings deposited on Si and the bulk-W samples exposed to D plasmas changing the ion energy.

| | no bias | 100 [V] | 200 [V] | 300 [V] | Type |
|---|---|---|---|---|---|
| b-W | none | yes | yes | yes | spongy, jagged and ripple-like |
| c-W | none | yes | yes | yes | ripple-like |
| a-W | none | none | yes | yes | hole (200 V) and ripple-like (300 V) |
| p-W | none | none | none | none | – |

### 3.2. Blister formation

SEM analysis of the compact a-W and c-W films deposited on flat Si showed the formation of micrometric-sized blisters, while no such features developed on the p-Ws. SEM analysis highlighted a reduction of blisters size by increasing the bias voltage, as can be observed from Fig. 7, particularly if one compares the exposure performed at 300 V to that where no bias is applied. For all the exposures and W morphology, blisters are μm-sized, the sole exception being the a-W exposed at 300 V, were much smaller blisters (nm-sized) were observed.

Blisters are also seen to strongly depend on the substrates properties. In particular, the c-W films deposited on rough W did not show any blister. The same also occurs for c-W deposited on mirror-polished Gr. However, for the c-W deposited on mirror-polished W and exposed to floating potential, the development of micrometer-sized blisters on the surface was observed, as shown in Fig. 8. The inset in the figure highlights corresponding AFM topographies on different spot of the sample, which allow to better appreciate the strong zone dependence of the blister size and shape. AFM and SEM measurements allow to appreciate the strong qualitative differences between blisters formed on the c-W deposited on mirror-polished W and flat Si (cfr. Fig. 7). On the one hand, one sees that blisters on flat Si appear to be higher in number and much more uniformly distributed. On the other hand, for the c-W deposited on mirror-polished W, blisters with different shape and height appear on top of the surface, with regions characterised by a strong coalescence of small-sized bubbles. A summary of blisters observed on the samples exposed in this work is reported in Table 5.

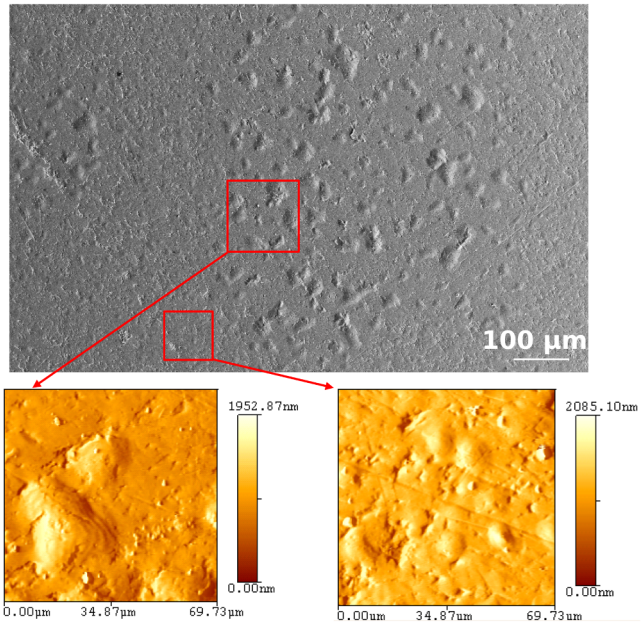


**Fig. 8.** SEM image of the blisters development after the plasma exposure on the c-W film deposited on mirror-polished W. The red insets highlight zone where AFM measurements were performed.

**Table 5**
Summary of the blisters observed on the surface of the samples exposed in this work. A dash denotes the fact that a particular sample was not exposed in the reported experimental condition.

| | | no bias | 100 V | 200 V | 300 V |
|---|---|---|---|---|---|
| | b-W | none | none | none | none |
| c-W | W mirror | yes | – | – | – |
| | W rough | none | – | – | – |
| | flat Si | yes | yes | yes | yes |
| | a-W | yes | yes | yes | yes |
| | p-W | none | none | none | none |

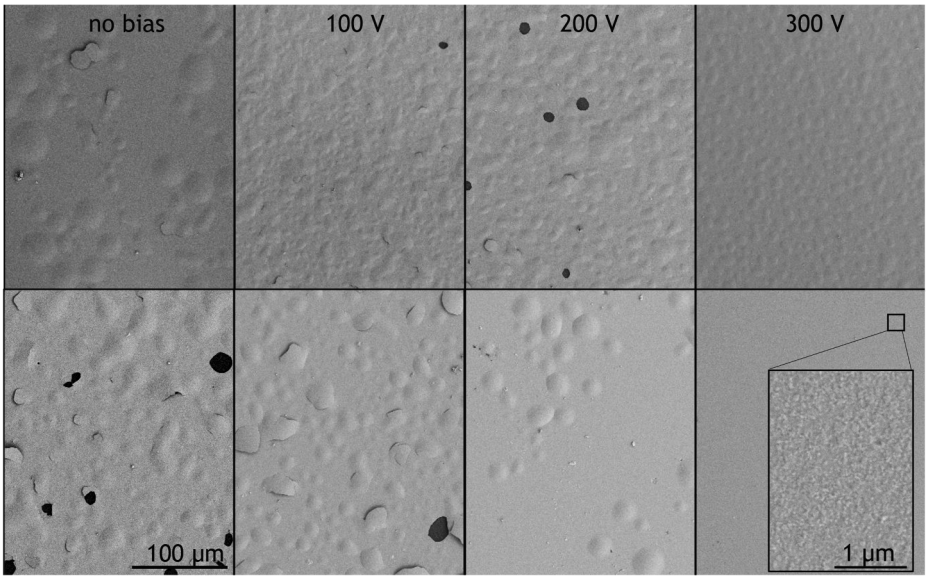


**Fig. 7.** SEM plain view showing the evolution of the blisters size, shape and number as a function of the applied bias voltage for the c-W (top row) and a-W (bottom row) coatings deposited on Si. The inset for the a-W exposed at 300V shows, in this case, blisters are much smaller (nanometric-sized).

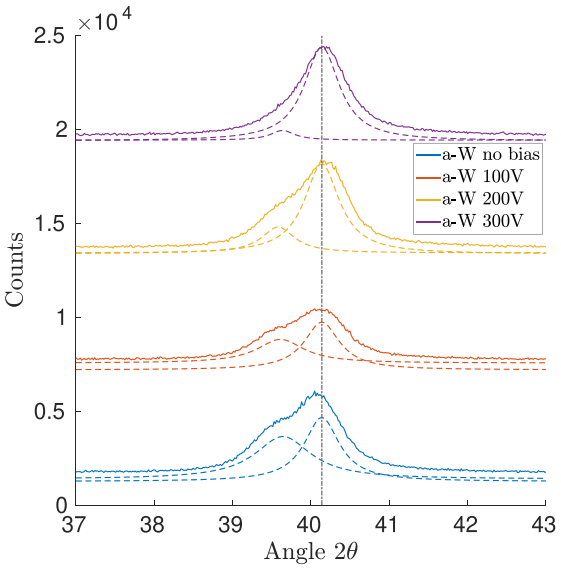


**Fig. 9.** XRD diffractograms of the exposed a-W samples. For each diffractoraph, the dashed lines denote the two lorentzian functions used to fit the data. One sees that the intensity of the lorentzian associated with the amorphous character of the a-W morphology progressively reduce. The dashed vertical line denotes the diffraction angle which corresponds to the ⟨110⟩ crystalline orientation of $\alpha$-W.

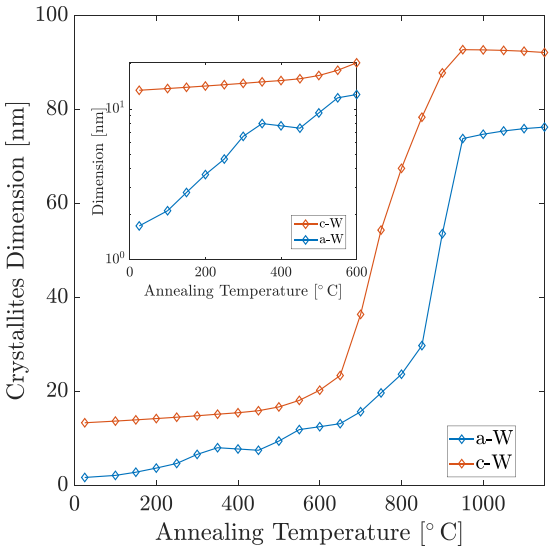


**Fig. 11.** Mean crystallite size for the a-W and the c-W as a function of the annealing temperature as computed from XRD measurements using the Scherrer's formula. The inset shows that in the temperature range 0 ÷ 600° the mean crystallite size of the c-W is almost constant, while it increases for the a-W already for relatively low annealing temperatures.

### 3.3. Crystallisation dynamics of a-W films

In the previous sections, we investigated the effect of the plasma flux with respect to the evolution of nanostructures and blisters. The plasma carries not only particles, but also energy which can have important effects on the W layer. Because of their amorphous-like structure (crystallite dimensions of few nanometers [28]) far from thermodynamic equilibrium, the a-W films are very sensitive with respect to temperature. Indeed, it is reported that vacuum annealing at 450–500 °C it is enough to induce the crystallization of the a-W film [35].

To investigate the impact of the plasma on the crystallinity of the a-W films, XRD measurements were performed on the exposed a-W samples with bias 0 ÷ 300 V. The diffractograms are shown in Fig. 9. It can be noted that all the spectra are characterized by a dominant peak located at $2\theta \simeq 40.1°$ and a shoulder. The peak is associated with the ⟨110⟩ crystalline direction of $\alpha$-W and it is due to the c-W crystalline adhesion layer [28]. The shoulder located to the left of the main peak, at about 39.6° is related to the broad amorphous band typical of the a-W morphology [28]. A fit, reported in Fig. 9, of the acquired spectra was performed using the sum of two Lorentzian functions; to account for the presence of the c-W interlayer, whose properties do not change during plasma exposures, one of the two Lorentzian was given a fixed peak position and FWHM, corresponding to those measured on an as-deposited c-W [28]. It can be noted that increasing the bias voltage, the shoulder progressively disappears and at 300 V only a small contribution remains. This analysis points to the fact that a crystallisation of the a-W has occurred during the exposures performed at the highest energy. Cross sectional SEM analysis of the exposed samples is reported in Fig. 10. It can be noted that increasing bias voltage up to 100 V results in a slight change of the morphology. At 200 V a columnar-like morphology appears. At 300 V the formation of the crystallised nanolayers is evident indicating a crystallisation of the a-W film. Due to the amorphous nature of the coatings the crystallisation is likely to happen at much lower temperatures compared with microcrystalline bulk W and compatible with the exposure temperatures.

To better address this point a dedicated annealing campaign has been performed with the aim of better characterise the crystallisation and recrystallisation dynamics of both a-W and c-W films. The films were deposited on quartz slides. No c-W interlayer was added on these substrates before depositing the a-W films. The annealings were performed in high vacuum ($10^{-6}$ Pa) varying the temperature in the range 100° ÷ 1250 °C in 50 °C increments, the dwell time set was one hour. Fig. 11 shows the mean crystallite size of a-W and c-W films as a function of the annealing temperature, as computed from XRD measurements using the Scherrer's formula applied to the peak associated with the ⟨110⟩ crystalline orientation of $\alpha$-W. It is worth to note that peak broadening of the XRD spectra is affected by the effects of the strain as well as the crystallite size [36]. Thus the use of the Scherrer method, that neglects the broadening contribution related to stresses may lead to an underestimation of the crystallite sizes. Crystallite dimension of c-W film does not appreciably change in the range 20 ÷ 650 °C, the mean crystalline dimension remains about 15 nm typical of physical vapor deposited films. At 650 °C a rapid recrystallization of the film occurs, the mean crystallite size from raised

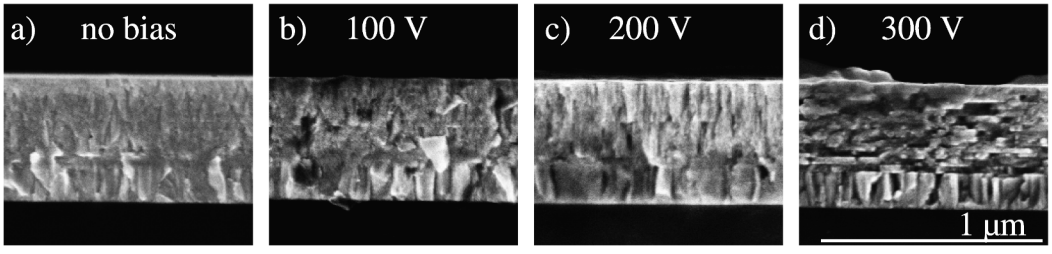


**Fig. 10.** SEM cross-sections of the a-W coatings after the exposures at no bias a), 100 b), 200 c) and 300 V d).

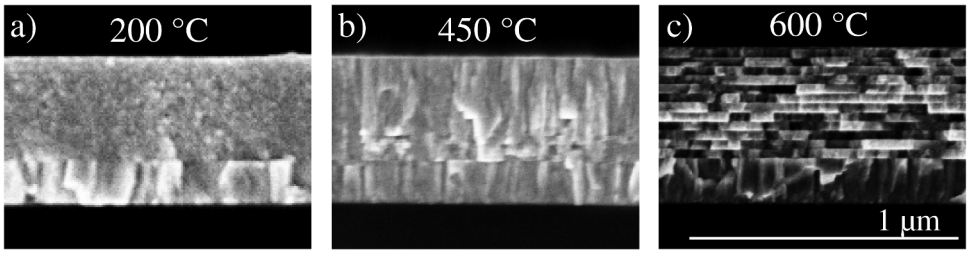


**Fig. 12.** Cross-sectional morphology obtained by SEM analysis of the a-W annealed at 200° a), 450° b) and 600° C c).

from 15 nm to 90 nm (that is the limit dimension appreciable with the Scherrer's formula). This value of recrystallization temperature is lower with respect to the one of microcrystalline W (about 1000 °C), this difference has to be ascribed at the nanocrystalline nature of c-W film. Due to their amorphous structure, the a-W films are even more sensible with respect to temperature than c-W films. The film starts to crystallise already at low temperatures (200 ÷ 300 °C). The growth is linear up to 650 °C going from 2 nm to 15 nm and is related to the grow of the crystalline domains and grain refinement from low energy defects such as dislocations. Above this temperature a sudden increase in crystallinity, from 15 nm up to 80 nm, occurs due to recrystallisation of the film similarly to what happened in c-W films. For both the a-W and c-W at temperatures above 1000 °C, the crystallite size rises with a little slope. A second session of annealings at 200 °C, 450° and 600° was performed on the a-W films deposited on Si with the same features of the exposed samples (c-W as interlayer) to perform SEM cross-section analysis, see Fig. 12. It can be noted that, coherently with the changes in crystallinity, the cross-sectional morphology changes already at 200°, if compared to that of the as-deposited a-W reported in Fig. 1. These changes become more evident at 450°, were a columnar-like growth, akin to that of the c-W morphology, is promoted (cfr. Fig. 1). At 600 °C, a peculiar layered structure develops. Each layer has a thickness of ~40 nm, and a morphology similar to the c-W interlayer, looking like a crystallisation layer by layer. The presence of such nanolayers is probably connected with the pulsed regime of the laser as well as with the movement of the ablation target during the deposition process. It is worth noting that due to the Si cleavage technique, the features of the cross section are influenced by the mechanical properties of the film (i.e. its ductility). W, due to its high ductile-to-brittle transition temperature, is quite fragile. Thus, every single W layer gets singularly broken during the cleavage resulting in a "rough" and irregular cross section. Future investigations regarding the impact of different cutting procedures (e.g. Focused Ion Beam cut) on the cross-sectional morphology will be the subject of a future work.

## 4. Discussion

### 4.1. Nanostructures formation

The formation of surface nanostructures is an important aspect to be considered for tokamaks operation. Indeed, as reported by [7], surface morphology changes at the nanoscale can lead to degradation of material properties as well as to enhanced erosion. Furthermore, in [7] a large surface concentration of D observed by Nuclear Reaction Analysis has been claimed to be correlated with the development of surface nanostructures. It has also been shown that surface modifications can lead to enhanced hydrogen retention [37].

The nanostructures observed after divertor-like exposure possess precise features. Xu et al. [9] report on the strong correlation between the nanostructure type and the crystalline grain orientation on Plansee W after the exposures to a high-flux ($10^{24}\,m^{-2}s^{-1}$) D plasma, at an overall fluence of $7 \times 10^{26}\,m^{-2}$. The ion energy was fixed to ~38 eV. In that study, three main types of surface nanostructures were identified: ripple, spongy and jagged. These last two were seen to form on those grains with a surface normal orientation directed along the ⟨100⟩ and ⟨111⟩ directions. The ripple nanostructure, instead, develops on those grains with other crystalline orientations. As reported in literature, two different mechanisms can contribute to the formation of surface nanostructures. In [8], their development on polycrystalline W exposed to a low energy (≃ 38 eV) high flux deuterium plasma ($>10^{24}\,m^{-2}s^{-1}$, for an overall fluence of $10^{26}\,m^{-2}$) has been correlated with the build-up of the D concentration near the surface, leading to a stress field. The high stress stored in the subsurface induces surface reconstruction. In addition the stress field hinders the diffusion of D toward the bulk, so that the D atoms cluster in nanocavities close to the surface causing the cyclic process of trap-mutation and dislocation loop punching and gliding, finally resulting, especially for the ⟨111⟩ and ⟨100⟩ orientations, in the formation of nanostructures on the top surface. In our work, we see a nanostructures development on the surface of both Plansee (bulk) W and compact W films (both c-W and a-W) deposited on Si after the exposures to medium D fluxes ($\simeq 5 \times 10^{20}\,m^{-2}s^{-1}$) of GyM for an overall fluence of $\sim 6 \times 10^{24}\,m^{-2}$, if the energy of the impinging ion species is sufficiently high (≳ 100 eV). The nanostructures obtained after the exposures performed in GyM show the same morphologies of the nanostructures obtained in literature under divertor-like conditions (see Fig. 5). Indeed, considering the Plansee (bulk) W, the formation of the same spongy, jeagged and ripple-like structures is seen to develop. The c-Ws showed the formation of only the ripple-like nanostructure, in agreement with the fact that XRD measurements show that the preferential crystalline orientation is ⟨110⟩. From these observations we can state that the formation mechanisms are the same for tungsten exposed at divertor-like plasmas or CXN-like ion fluxes. The use of energetic ion induces the development of such nanostructures at much lower fluence values ($10^{24}\,m^{-2}$ vs $10^{26}\,m^{-2}$). In the present case the high energy (100 ÷ 300 eV) of the impinging species is probably enhancing the stress field present in the films leading to an early development of the nanostructures even at medium fluxes ($\sim 10^{20}\,m^{-2}s^{-1}$) and fluences ($6 \times 10^{24}\,m^{-2}$).

In addition, since in the case of the exposures performed at 300 V we are over the sputtering threshold, sputtering effects could contribute to the formation and evolution of surface nanostructures, as reported by Škereň et al. in [38], at least for polycrystalline bulk metals with nanometric-sized grains. The authors report that, after irradiation at energies well above the sputtering threshold, the formation of ripples at the nanoscale might be explained as due to the local variation of the sputtering yield which in turn is related to the crystalline orientation of the grains and the local ion incidence angle [38].

To further investigate the nature and the stability of the formed nanostructures, dedicated annealing experiments were performed on the c-W morphology exposed at 300 V in the same home-made furnace as that described in Section 3.3. The dwell time was fixed to 4 hours and only the temperature was changed. Fig. 13 shows SEM plain-views of the surface morphology for the two annealing temperatures of 600 °C and 750 °C. The surface nanostructures are stable at 600 °C. A complete disappearance of the ripple nanostructure takes place for the annealing temperature of 750 °C. The modification has bee related to the recrysallisation of the c-W films that, has reported in the previous section and in [39], is seen to occur in this temperature range.

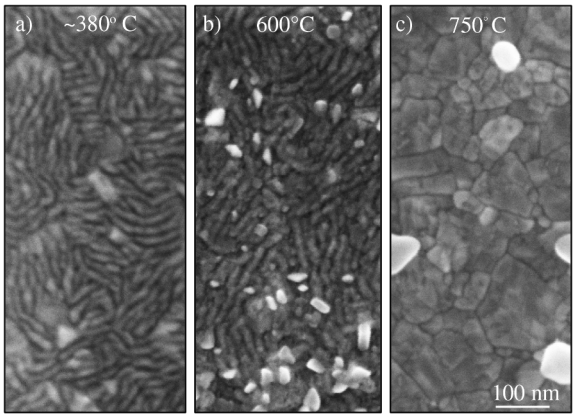


**Fig. 13.** SEM plain-views (a–c) showing the evolution of the ripple nanostructures after a pure thermal load. Figure a) refers to the exposed c-W at 300 V. In this case, the surface temperature (~380 °C) is estimated according to the discussion made in Section 2.3.

Exploiting the peculiarity of our nanostructured films we have the chance to study the role of crystallinity in the formation of surface nanostructures. The extension in plain of the nanostructures is seen to be related to the grain size of W (micrometric domains for bulk-W and nano domains for c-W). The presence of a crystalline grain seems to be a strong requirement for the formation of the nanostructures. In fact, the amorphous a-W films do not show any formation of nanostructures at low energy (below ~200 eV) when the film maintained its original amorphous morphology (cfr. Section 3.3). This hypothesis is further supported by the fact that the p-W, which do not have a crystalline structure [28], did not developed any nanostructure. The development of nanostructures on a-W film takes place only after a consistent crystallization of the film.

Nanostructures formation on c-Ws and a-Ws films deposited on bulk Plansee W was also studied in [13] after exposures to a flux of $1.4 \times 10^{24}\,m^{-2}s^{-1}$, fluence of $2.5 \times 10^{26}\,m^{-2}$ and an applied bias voltage of − 40 V. In that case for the c-W also jagged-like nanostructures develop on the surface in addition to the already observed ripple structures. This additional morphology could be explained as due to the fact that the c-W film in [13] was grown on Plansee W and thus might present additional W crystallographic orientation other than the ⟨110⟩, as detailed in [17]. As discussed before, these additional grain orientations favour the growth of different types of nanostructures. The a-W films of [13] also developed ripple-like surface nanostructures but with a random orientation. This could be ascribed at the effect of the higher flux and fluence respect to the present experiment, in addition a partial recrystallisation migth occur since in [13] the surface temperature was kept to 250 °C which we showed (cfr. Section 3.3) to be sufficient to initiate a first stage of recrystallisation.

### 4.2. Blister formation

Blisters formation on coatings is an important aspect to be considered. Indeed, tokamaks are inherently pulsed device and are characterised by mixed-material first wall, so that the development of layered deposits on top of the pristine first-wall might occur. In this case, the accumulation of D gas at the interface can happen, resulting possibly in a delamination of the layer leading to the generation of dust particles which can cause plasma termination. The phenomena was indeed observed in the Large Helical Device, as reported in [20].

In our work, we showed that the morphology of the W coatings play a major role in suppressing blistering. Indeed, the p-W films did not blister under any of the exposures conditions considered here, as already reported in [39]. This might be due to the open morphology of this coating, which lead to a preferential desorption of $D_2$ gas trapped in the bulk of the coating. Furthermore, we showed that blistering on compact (columnar and amorphous) deposited on flat Si occurs in any of the considered exposure conditions. The shape and size of the blisters are, however, influenced by the applied bias voltage. In particular, we showed that smaller blisters are found at higher energies, and vice versa. This behavior is different with respect to bulk W where smaller blisters are favored by low energy [19].

As summarised in Table 5, the blistering is also influenced by the surface roughness. In particular, in this work we showed that blisters can be strongly suppressed by surface roughness. Blistering is observed to occur for the W coatings deposited on flat Si and mirror-polished W, but are suppressed for rough substrates. This result finds confirmation from literature [18,40], where however blistering suppression was observed on bulk materials and on powder metallurgy W, as in our case, for coatings.

Combining our results with literature data, we can say that the mechanism for blistering on coatings and on bulk metals are different. Indeed, for blistering on bulk metals under low energy plasma (<100 eV) fluxes below $10^{23}\,m^{-2}s^{-1}$, the mechanisms of crack growth and loop punching are often mentioned and refer to a plastic deformation due to D supersaturation [14]. Considering W, during the implantation of low energy deuterium ions, if the incident flux is higher than the rate of D diffusion out of the implantation range, combined with the low solubility of D in W, then a high D concentration (supersaturation) in the near surface results. This leads to stresses that are relaxed by blistering. For coatings, blistering is due to a different mechanism. In [41], blistering on W films morphologies similar to those considered in the present work was reported after low energy divertor-like (fluxes $\sim 10^{24}\,m^{-2}s^{-1}$ for an overall fluence of $\sim 10^{26}\,m^{-2}$), plasma exposures. These studies revealed that blistering is likely to be related to the accumulation of the D at the Si – W interface. The plausibility of this mechanism is confirmed from our exposures, as can be noted from Fig. 14, where we show a SEM plain view of the a-W coating locally delaminated due to blister-induced stresses. One readily observes the growth of spherical bubbles which can reach the ~1 μm size before coalescence with other, similar, blisters occurs. The process of blister growth and coalescence continues until the pressure inside is sufficiently high to promote delamination of the coating.

In addition to coating's morphology, the roughness of the substrates and the coating's thickness, blistering can be also influenced by the residual stress at the coating-substrate interface. As regard this latter aspect, in [17] D retention in W films deposited by Magnetron Sputtering (MS) on mirror-polished Plansee W and Si is investigated by Nuclear Reaction Analysis, after exposures to a D plasma in PlaQ with fluences in the range of $10^{24}\,m^{-2}s^{-1}$ and ion energy of 38 eV. The

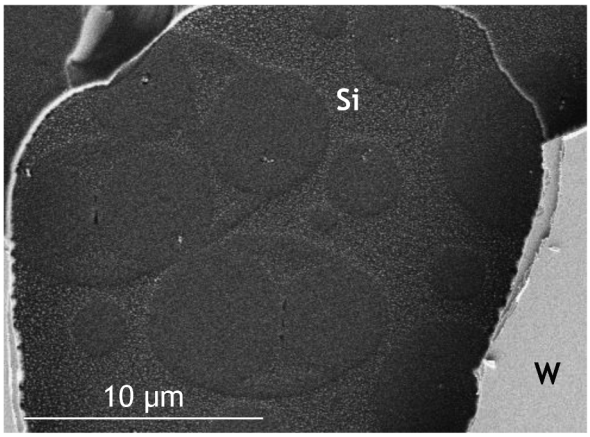


**Fig. 14.** SEM plain view showing the details of blister formation due to the accumulation of D at the Si – W interface.

morphology of the W coatings grown by MS is very similar to that of our c-Ws. Blistering was observed only for the W film grown on Plansee W. This result can be explained by a residual-stress argument. Indeed, it is known (e.g. [42]) that residual stresses at the film-coating interface strongly depend on *i*) the film and substrate materials and *ii*) on the deposition technique: *i*) are due to thermal stresses, while *ii*) strongly depend on the energy of the species deposited on the substrate. The final state of residual stress depends on which of these two mechanisms dominate over the other. For high energy of the impinging species during the deposition (as it happens for PLD-deposited coatings) the latter usually dominates over the former. It is likely that the process of blister growth is strongly inhibited by tensile stresses, while it is favoured by a compressive stress. Indeed, in our case the growth of a blister induces a compressive stress that adds to the already compressed films. This argument applies, of course, for the compact coatings (c-W and a-W) where the energy of the species deposited on the substrate after the ablation process is high. To relax the pressure-induced stress, the film buckle leading to its detachment from the interface. The opposite happens in the case of a tensile residual stress (as it occurs for films deposited by MS), where the strain induced by the blister is inhibited.

## 5. Conclusions

In this work, bulk W and nanostructured W coatings with different morphology and structure were exposed to a particle flux similar to those of CXNs at the main chamber of present-day tokamaks and expected in ITER. We found that, thanks to the high energy regime of the impinging species, the exposed W (bulk and nanostructured) is modified both at the nano and at the micro scale. The development of surface nanostructures was observed at a fluence that is two order of magnitude lower than the one typical of the divertor region in tokamaks. Moreover, morphology and crystallinity of the W coatings determine the features and even the development of the nanostructures. Porous W films inhibit nanostructure formation. In addition, we found that the presence of crystalline domains, at least at the nanometric level, is a mandatory requirement for the development of the nanostructures. The development of micrometric-sized blisters was observed for the compact W coatings. Their number, size and shape are found to strongly depend on the film morphology, substrates properties, residual stresses and energy of the ion species.

## CRediT authorship contribution statement

**M. Sala:** Writing - original draft, Writing - review & editing, Formal analysis, Investigation, Visualization. **A. Uccello:** Writing - review & editing, Resources, Investigation. **D. Dellasega:** Writing - review & editing, Resources, Methodology. **M. Pedroni:** Resources, Investigation. **E. Vassallo:** Resources, Investigation. **M. Passoni:** Conceptualization, Supervision, Project administration, Funding acquisition.

## Declaration of Competing Interest

The authors declare that they have no known competing financial interests or personal relationships that could have appeared to influence the work reported in this paper.

## Acknowledgments

The authors wish to thank C. Conti and A. Pezzoli. This work has been carried out within the framework of the EUROfusion Consortium and has received funding from the Euratom research and training programme 2014–2018 and 2019–2020 under grant agreement No 633053. The views and opinions expressed herein do not necessarily reflect those of the European Commission

## References

[1] O. Gruber, et al., Compatibility of iter scenarios with full tungsten wall in asdex upgrade, Nuclear Fusion 49 (11) (2009) 115014.
[2] R. Neu et al., Tungsten experiences in ASDEX upgrade and JET, in: 2013 IEEE 25th Symposium on Fusion Engineering (SOFE). IEEE, 2013.
[3] S. Brezinsek, et al., Plasma–wall interaction studies within the EUROfusion consortium: progress on plasma-facing components development and qualification, Nuclear Fusion 57 (11) (2017) 116041.
[4] E. Fortuna-Zaleśna, et al., Studies of dust from JET with the ITER-like wall: Composition and internal structure, Nuclear Materials and Energy 12 (2017) 582–587.
[5] A. Baron-Wiechec, et al., First dust study in jet with the iter-like wall: sampling, analysis and classification, Nuclear Fusion 55 (11) (2015) 113033.
[6] M. Mayer, et al., Erosion and deposition in the jet divertor during the first ilw campaign, Physica Scripta 2016 (T167) (2016) 014051.
[7] M.H.J. 't Hoen et al., Surface morphology and deuterium retention of tungsten after low- and high-flux deuterium plasma exposure, Nuclear Fusion 54 (8) (2014) 083014.
[8] H.Y. Xu, et al., Observations of orientation dependence of surface morphology in tungsten implanted by low energy and high flux d plasma, Journal of Nuclear Materials 443 (1–3) (2013) 452–457.
[9] H.Y. Xu, et al., Enhanced modification of tungsten surface by nanostructure formation during high flux deuterium plasma exposure, Journal of Nuclear Materials 447 (1–3) (2014) 22–27.
[10] Y.Z. Jia, et al., Nanostructures and pinholes on w surfaces exposed to high flux d plasma at high temperatures, Journal of Nuclear Materials 463 (2015) 312–315.
[11] Y.Z. Jia, et al., Subsurface deuterium bubble formation in w due to low-energy high flux deuterium plasma exposure, Nuclear Fusion 57 (3) (2016) 034003.
[12] M. Zibrov, et al., Deuterium trapping and surface modification of polycrystalline tungsten exposed to a high-flux plasma at high fluences, Nuclear Fusion 57 (4) (2017) 046004.
[13] M.H.J. 't Hoen et al., Deuterium retention and surface modifications of nanocrystalline tungsten films exposed to high-flux plasma, Journal of Nuclear Materials 463 (2015) 989–992.
[14] V.Kh. Alimov, et al., Depth distribution of deuterium in single- and polycrystalline tungsten up to depths of several micrometers, Journal of Nuclear Materials 337–339 (2005) 619–623.
[15] V.Kh. Alimov, et al., Temperature dependence of surface topography and deuterium retention in tungsten exposed to low-energy, high-flux d plasma, Journal of Nuclear Materials 417 (1–3) (2011) 572–575.
[16] M.Y. Ye, et al., Blister formation on tungsten surface under low energy and high flux hydrogen plasma irradiation in NAGDIS-i, Journal of Nuclear Materials 313–316 (2003) 72–76.
[17] P. Wang, et al., Deuterium retention in tungsten films deposited by magnetron sputtering, Physica Scripta 2014 (T159) (2014) 014046.
[18] Armin Manhard et al., Blister formation on rough and technical tungsten surfaces exposed to deuterium plasma, Nuclear Fusion, 57 (12) (2017) 126012.
[19] K. Ouaras, et al., Tungsten blister formation kinetic as a function of fluence, ion energy and grain orientation dependence under hydrogen plasma environment, Journal of Fusion Energy 37 (2–3) (2018) 144–153.
[20] M. Shoji, et al., Studies of dust transport in long pulse plasma discharges in the large helical device, Nuclear Fusion 55 (5) (2015) 053014.
[21] Y. Marandet, et al., Assessment of tungsten sources in the edge plasma of WEST, Journal of Nuclear Materials 463 (2015) 629–633.
[22] N. Mellet et al., Multiscale modelling of sheath physics in edge transport codes, in: 26th IAEA Fusion Energy Conference, 2016.
[23] Y. Ueda, et al., PSI issues at plasma facing surfaces of blankets in fusion reactors, Journal of Nuclear Materials 313–316 (2003) 32–41.
[24] R. Behrisch, et al., Material erosion at the vessel walls of future fusion devices, Journal of Nuclear Materials 313–316 (2003) 388–392.
[25] M. Mayer, et al., Tungsten surface enrichment in EUROFER and fe-w model systems studied by high-resolution time-of-flight rutherford backscattering spectroscopy, Nuclear Materials and Energy 17 (2018) 147–151.
[26] R. Caniello, et al., Erosion yield and w surface enrichment of fe-w model system exposed to low flux deuterium plasma in the linear device GyM, Nuclear Materials and Energy 10 (2017) 9–16.
[27] D. Alegre, et al., A parametric study of helium retention in beryllium and its effect on deuterium retention, Physica Scripta T170 (2017) 014028.
[28] D. Dellasega, et al., Nanostructured and amorphous-like tungsten films grown by pulsed laser deposition, Journal of Applied Physics 112 (8) (2012) 084328.
[29] R. Mateus, et al., Helium load on w-o coatings grown by pulsed laser deposition, Surface and Coatings Technology 355 (2018) 215–221.
[30] C. Ruset, et al., Development of w coatings for fusion applications, Fusion Engineering and Design 86 (9–11) (2011) 1677–1680.
[31] E. Fortuna-Zalesna, et al., Post mortem analysis of a tungsten coated tile from the outer divertor strike point region of ASDEX upgrade, Nuclear Materials and Energy 9 (2016) 128–131.
[32] M. Rasinski, et al., High resolution scanning transmission electron microscopy (HR STEM) analysis of re-deposited layer on ASDEX upgrade tile, Fusion Engineering

and Design 86 (9–11) (2011) 1753–1756.
[33] G. Granucci et al., The new linear plasma device gym at ifp-cnr, in: 36th EPS Conference on Plasma Physics, 2009.
[34] K. Sugiyama, et al., Sputtering of iron, chromium and tungsten by energetic deuterium ion bombardment, Nuclear Materials and Energy 8 (2016) 1–7.
[35] D. Dellasega, et al., Tungsten oxide nanowires grown on amorphous-like tungsten films, Nanotechnology 26 (36) (2015) 365601.
[36] G. Antar, J. Ali, C. Madi, M. Noun, V. Rohde, M. Roumié, A.J. Said, J. Younes, The properties of the tungsten coating on fine grain graphite using pulsed laser deposition, Fusion Engineering and Design 148 (2019) 111261.
[37] M.H.J. 't Hoen et al., Strongly reduced penetration of atomic deuterium in radiation-damaged tungsten, Physical Review Letters, 111(22) (2013).
[38] T. Škereň, et al., Ion-induced roughening and ripple formation on polycrystalline metallic films, New Journal of Physics 15 (9) (2013) 093047.
[39] Andrea Pezzoli, Tungsten-based coatings for magnetic fusion research: damage and hydrogen retention, PhD thesis, 2017.
[40] D. Nishijima, H. Iwakiri, K. Amano, M.Y. Ye, N. Ohno, K. Tokunaga, N. Yoshida, S. Takamura, Suppression of blister formation and deuterium retention on tungsten surface due to mechanical polishing and helium pre-exposure, Nuclear Fusion 45 (7) (2005) 669–674.
[41] M.H.J. 't Hoen et al., Deuterium retention and surface modifications of nanocrystalline tungsten films exposed to high-flux plasma, Journal of Nuclear Materials 463 (2015) 989–992.
[42] J. Xiong, et al., Effect of processing conditions and methods on residual stress in CeO2 buffer layers and YBCO superconducting films, Physica C: Superconductivity 442 (2) (2006) 124–128.